Optics and Lasers in Engineering 162 (2023) 107390

Contents lists available at ScienceDirect

Optics and Lasers in Engineering

journal homepage: www.elsevier.com/locate/optlaseng

Design of orthogonal tunable spatial heterodyne spectrometer based on prism dispersion

Yixuan Li[a,b,*], Yu Huang[a,*], Yunhan Wu[a,b], Haochen Li[a,b], Xiaohu Yang[a], Zhanfeng Li[a], Zihui Zhang[a]

[a] Changchun Institute of Optics, Fine Mechanics and Physics, Chinese Academy of Sciences, No. 3888, Dongnanhu Road, Changchun, Jilin 130033, China
[b] University of Chinese Academy of Sciences, Beijing 100049, China

ARTICLE INFO

Keywords:
Tunable
Spatial heterodyne spectroscopy
Orthogonal

ABSTRACT

In our paper, we present a new design for an orthogonal tunable spatial heterodyne spectrometer (SHS) and a method to construct a spatial heterodyne base on the prism. Our design makes the radial plane of the tuned shaft orthogonal to the plane of the folding-path thus one can quickly tune the system to an arbitrary spectral range without additional moving parts. In addition, the Prism-Mirror instead of grating in SHS is used to avoid lateral confinement, which causes the resolving power to be overestimated, in the existing SHS based on gratings.

1. Introduction

The concept of spatial heterodyne spectroscopy (SHS) was first proposed by Dohi and Susuki of Osaka University in 1971 [1]. The spectrometer based on this technology can obtain high spectral resolution in a small wavelength range centered on a certain wavelength, which has been proved to have high potential in various optical measurements. It is widely used in weak signal measurement and ultra-high resolution spectral line characteristic peak detection, including interstellar medium remote sensing [2], observation of extreme changes in the Earth's ionosphere [3], monitoring of hydroxyl radicals in the Earth's middle atmosphere [4] and laser induced breakdown spectroscopy (LIBS) [5–7]. Since SHS has no moving mirror in the measurement, this characteristic enables it to be used for the measurement of pulse source [8,9]. The structure of SHS is close to that of the Michelson interferometer, the difference is that the two mirrors on both arms are replaced by two diffraction gratings placed at the conjugate angle θ_L (Littrow angle). The simplest SHS structure is shown in Fig. 1. After the collimated incident light is split by the beam cube, it is incident on the grating surface at the same angle θ. After the +1 order diffraction light of the two gratings passes through the beam splitter prism again, the combined light is imaged to the surface of the detector through the imaging lens, forming a pattern similar to the Fissau interference fringe.

SHS makes full use of the spatial information of the detector to achieve higher spectral resolution by moving the equivalent zero-frequency position to the Littrow wavenumber position. However, the size and resolution of the detector are limited, which means that the number of interference fringes that the detector can collect is limited, too. Therefore, while SHS obtains the hyperspectral resolution, its bandwidth is difficult to cover a wide spectral range. However, in applications such as solar spectral irradiance remote sensing and atmospheric composition inversion, spectral remote sensing instruments with high spectral resolution and wide spectral range need to be considered. To meet this demand, tunable spatial heterodyne spectroscopy (TSHS) is proposed. To realize the tuning of SHS, in the case of the original SHS design (Fig. 1), one difficulty is how to align the inclination angles of two separated gratings with the same Littrow angle in the tuning process, and another difficulty is how to ensure the alignment of two gratings. Some ideas have been proposed in the literature, such as using one-mirror-one-grating layout [10] or placing two back-to-back glued gratings in a common out-folded optical path [11]. In the design of one-mirror-one-grating, diffraction only occurs on one arm, so the spectral resolution is only half; in the design of glued gratings, although diffraction occurs on two arms, the two gratings are glued back-to-back, and the alignment of the two gratings is very difficult. To solve this problem, Hungarian scholar Gergely Németh and American scholar Olivia R. Dawson both proposed a single grating scheme, but in the design of Gergely Németh, the optical path difference between the two arms along the optical axis is different, and an additional flat moving mirror is needed [12]. The design of Olivia R. Dawson needs two tunable mirrors, and there are still requirements for accurate and synchronous operation of moving parts [13,14]. Besides, Matthias Lenzne pointed out that the existing grating-based TSHS has the problem of wavefront and energy front separation, which are too optimistic to estimate its

* Corresponding authors at: Changchun Institute of Optics, Fine Mechanics and Physics, Chinese Academy of Sciences, No. 3888, Dongnanhu Road, Changchun, Jilin 130033, China.
E-mail addresses: liyixuan17@mails.ucas.edu.cn (Y. Li), hycnsss@163.com (Y. Huang).

https://doi.org/10.1016/j.optlaseng.2022.107390
Received 18 June 2022; Received in revised form 30 October 2022; Accepted 13 November 2022
Available online 9 December 2022
0143-8166/

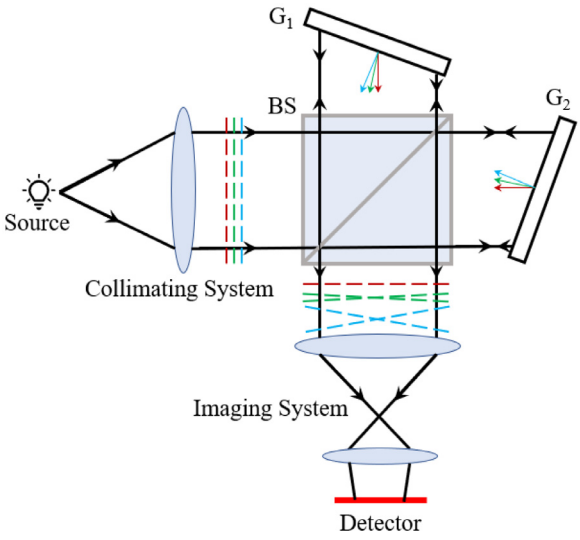

Fig. 1. The Simplest type of schematic diagram of Spatial Heterodyne Spectrometer. Arrows of different colors represent rays with different wavenumbers, and the dotted lines of different colors illustrate the corresponding tilted wavefronts of the two arms. The Fissau interference fringe of the tilted plane waves is recorded by a CCD/CMOS.

spectral resolution [11]. Therefore, there are two key problems to be solved: one is how to ensure that the optical path difference (OPD) between the two arms along the optical axis is zero in the tuning process in the single moving mirror TSHS structure; another one is how to avoid the problem of limited lateral interference.

2. Orthogonal TSHS design based on prism

To solve these problems, we have improved the design of the existing TSHS: a three-dimensional interference optical path structure is designed, in which the radial surface of the tuning shaft is orthogonal to the internal refractive path plane, to avoid the use of multiple moving parts; the feasibility of using a prism to construct spatial heterodyne was studied to solve the problem of limited lateral interference in existing SHS based on gratings.

2.1. Orthogonal stereo optical path

The conceptual drawing of the new design can be seen in Fig. 2. The main concept is to replace the plane mirror in one of the arms of a Sagnac-like interferometer with a roof mirror. Then we placed a roof-top mirror (RTM)into the common path to turn the beams outward parallel to each other. The parallel beam after the roof-top mirror reaches the dispersion system, and then the dispersion light returns to the beam splitter prism along the incident light path, and finally is transmitted to the detector surface and forms a high visibility interferogram. The tuning shaft is located on the grating or the mirror of the prism-mirror, and the radial surface of the shaft is orthogonal to the out-folded path plane. The tuning is realized by tilting the grating or mirror.

After the incident light passes through the collimating system, the bundled cube is divided into arm A and arm B (Fig. 2). Arm A contains a rectangular prism reflector, and arm B contains a hollow roof prism reflector. Fig. 3 shows the cross-section flip of the two-arm beams after passing through different optical components. The cross-sections of the two beams emitted parallelly from the roof mirror are symmetrical in both horizontal and vertical directions, and the two-arm beams will be emitted along the incident path after passing through the dispersion system. In other words, the transitions in any direction in the dispersion system are conjugate symmetry for the two-arm beams, so the dispersion system can be dispersed in any direction. If the radial plane of the tuning shaft is set to be orthogonal to the plane of the out-folded path, the OPD between the two arms along the optical axis (blue dot streak in Fig. 2) can always be zero in the tuning process.

In the interferometric optical system, we use the optical components of Thorlabs and Edmund, and the types and parameters are shown in Table 1. To obtain the best spectral performance, combined with the detector size and the aperture size of the system, we use two achromatic lenses to form a bi-telecentric imaging system with a magnification of 0.5 ×, Their focal lengths are 400mm (Thorlabs AC254-400-A-ML) and 200mm (Thorlabs AC254-200-A-ML) respectively.

2.2. Spatial heterodyne constructed by prism

Matthias Lenzne proposed that the existing SHS scheme was too optimistic about the estimation of spectral resolution [11]. For the existing SHS based on gratings, the limitation of the transverse interference region is not only determined by the coherent time τ of the incident light and the wavefront inclination $\Delta\theta$, but also related to the energy front inclination γ. This phenomenon is caused by the separation of the wavefront and the energy front of the grating diffraction light (Fig. 4a left). The monochromatic light is incident on the grating surface with Littrow angle θ_L, and the diffraction light of the grating +1 stage is also emitted with Littrow angle. They are parallel to each other, and the wavefront (yellow lines) must be perpendicular to the propagation direction of the light. However, for different positions of the beam cross-section, the optical path is different (the green region in Fig. 4a left). Currently, the deflection angle of the energy front of the diffraction light $\gamma = 2\theta_L > \Delta\theta$, and the deflection angle of energy front γ becomes the main factor limiting the transverse interference region. Compared with diffraction dispersion, refraction dispersion does not lead to the separation of the wavefront and energy front (Fig. 4a). The monochromatic light is incident at the Littrow angle to the dispersion system composed of refractive surface and mirror, and the reflected light is emitted at the same angle. For different positions of the beam cross-section, the optical path they experience is completely consistent (the green area in Fig. 4a right). Thus, using a prism as a dispersion element can avoid the problem of limited transverse interference in SHS. Fig. 4b shows that how to construct spatial heterodyne by prism-mirror, where the tuning axis is located on the mirror and can be tuned to any waveband by rotating the mirror.

For quasi-monochromatic light with coherent time τ, the transverse interference region x_g when the dispersion element is a grating and the transverse interference region x_p when the dispersion element is a prism are expressed as $c\tau / \tan\gamma$ and $c\tau / \tan\Delta\theta$, respectively. Fig. 4c shows the relationship between the wavefront and the energy front of the emitted light when the beam is incident at a non-Littrow angle. Spectral resolution $\Delta\lambda$ can be expressed as a function of transverse interference region x:

$$\Delta\lambda = 2d \cdot \left\{ \sin\left[\arcsin\left(\frac{\lambda}{2d}\right) + \arctan\left(\frac{\lambda}{2x}\right)\right] - \frac{\lambda}{2d} \right\} \quad (1)$$

where d is the grating constant, λ is the Littrow wavelength, and x is the transverse interference region. It can be seen that the prism-mirror can realize the construction of spatial heterodyne, thus avoiding the problem of transverse interference limitation caused by the separation of wavefront and energy front, and reconstructing the target spectrum with the best spectral resolution.

2.3. Resolving power

The incident angle of the two-arm beams to the dispersion system is φ_1, and the exit angle is φ'_1. Then the deflection angle of the beam after passing through the dispersion system $\gamma = |\varphi_1 - \varphi'_1|$, as shown in Fig. 4b. If the refractive index of the equilateral prism is $n(\sigma)$, then the deflection angle γ of incident light corresponding to wave number $\sigma_i = \sigma_0 + \Delta\sigma_i$

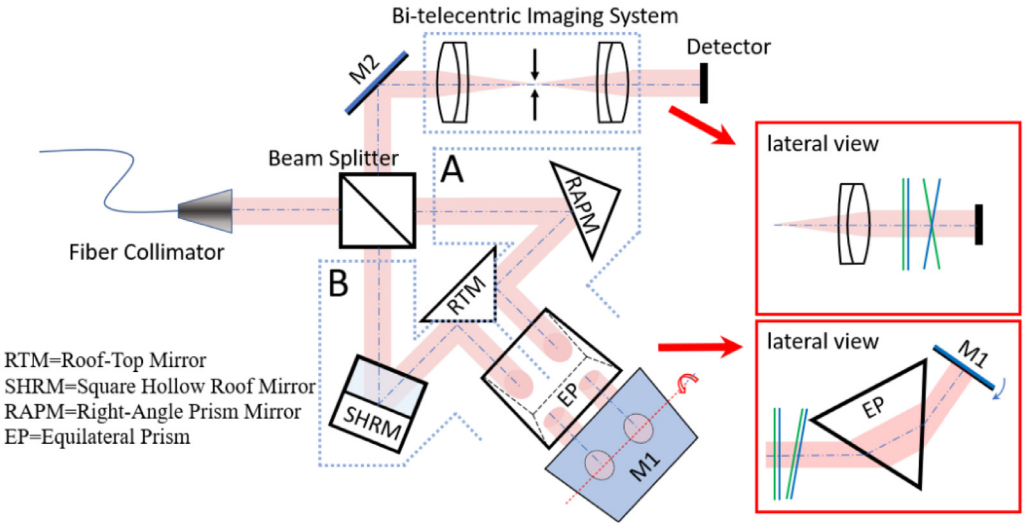

Fig. 2. Novel design of orthogonal tunable spatial heterodyne spectrometer based on the prism. The beam paths are folded out with a square hollow roof mirror (SHRM), right-angle prism mirror (RAPM), and roof-top mirror (RTM), and the SHRM is used to flip the B-arm beam along the vertical direction. The two beams incident at the same Littrow angle to the dispersion system composed of prism and plane mirror, and then the combined beam relays to the detector by a bi-telecentric imaging system. The aperture stop is equivalent to the aperture filter, which plays the role of a band-pass filter.

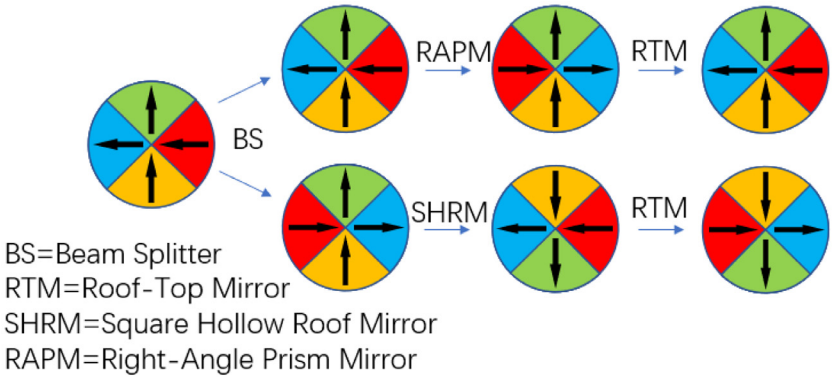

Fig. 3. Flip diagram of the cross-section of two arms incident light. The circle is the cross-section of the incident light, and the color block and arrow indicate the turnover of the cross-section. The figure shows that the horizontal direction is parallel to the refractive path plane outside the interference system. The horizontal direction is parallel to the external refraction plane of the interference system.

Table 1
Types and parameters of interference optical path system components.

Components	Types	Parameters
Beamsplitter Cube	Thorlabs BS013	1", 50:50, Non-Polarizing Cube
Plane Mirror	Edmund #68-334	50mm × 50mm, Prot. Silver, $\lambda/10$
Retroreflecting Hollow Roof Prism Mirrors	Thorlabs HRS1015-G01	1" × 1", Prot. Aluminum, $\lambda/4$
Right-Angle Prism Mirror	Thorlabs MRA25-G01	L = 25.0 mm, Prot. Aluminum, $\lambda/10$
Knife-Edge Roof Mirror	Thorlabs MRAK25-G01	L = 25.0 mm, Prot. Aluminum, $\lambda/10$
Equilateral Prism	Edmund #49-432	50mm, uncoated, N-SF11, $\lambda/4$

can be shown as:

$$\gamma\left(\sigma_i,\theta_{\sigma_0},n(\sigma_i),\varphi_1\right)=|\varphi_1-\varphi_1'|=\left|\varphi_1-\arcsin\left(n(\sigma_i)\sin\left(\alpha-\frac{\sin\left(\arcsin\left(n(\sigma_i)\sin\left(\alpha-\arcsin\left(\frac{\sin\varphi_1}{n(\sigma_i)}\right)\right)\right)+2\left(\theta_{\sigma_0}-\theta_{\sigma_i}\right)\right)}{n(\sigma_i)}\right)\right)\right| \tag{2}$$

Where α is the top angle of the prism, $\theta_{\sigma 0}$ is the Littrow angle corresponding to the wavenumber σ_0, which is also the tuning angle currently. $\theta\sigma$i is the Littrow angle corresponding to the wavenumber σi, which can be expressed as:

$$\theta_{\sigma_i}=\varphi_1-\alpha+\arcsin\left(n(\sigma_i)\sin\left(\alpha-\arcsin\left(\frac{\sin\varphi_1}{n(\sigma_i)}\right)\right)\right) \tag{3}$$

For a given substrate material and incident angle φ1, the relationship between the deflection angle of dispersive light $\gamma_i=\gamma(\sigma_i,\sigma_0)$ and the number of incident light σ_i and the tuning angle $\theta_{\sigma 0}$ is obtained.

For monochromatic light with wavenumber σ_i, the interference fringe spacing s_i is equal to

$$s_i=\frac{M}{4\cdot(\sigma_0+\Delta\sigma_i)\cdot\sin\gamma_i} \tag{4}$$

where M is the magnification of the imaging system. Assuming that for two wavenumbers (σ_0+σ_1) and (σ0+σ_2) the number of fringes over the width of the aperture must differ by at least 1/2, we can deduce the corresponding resolution criterion. This is based on the Rayleigh criterion:

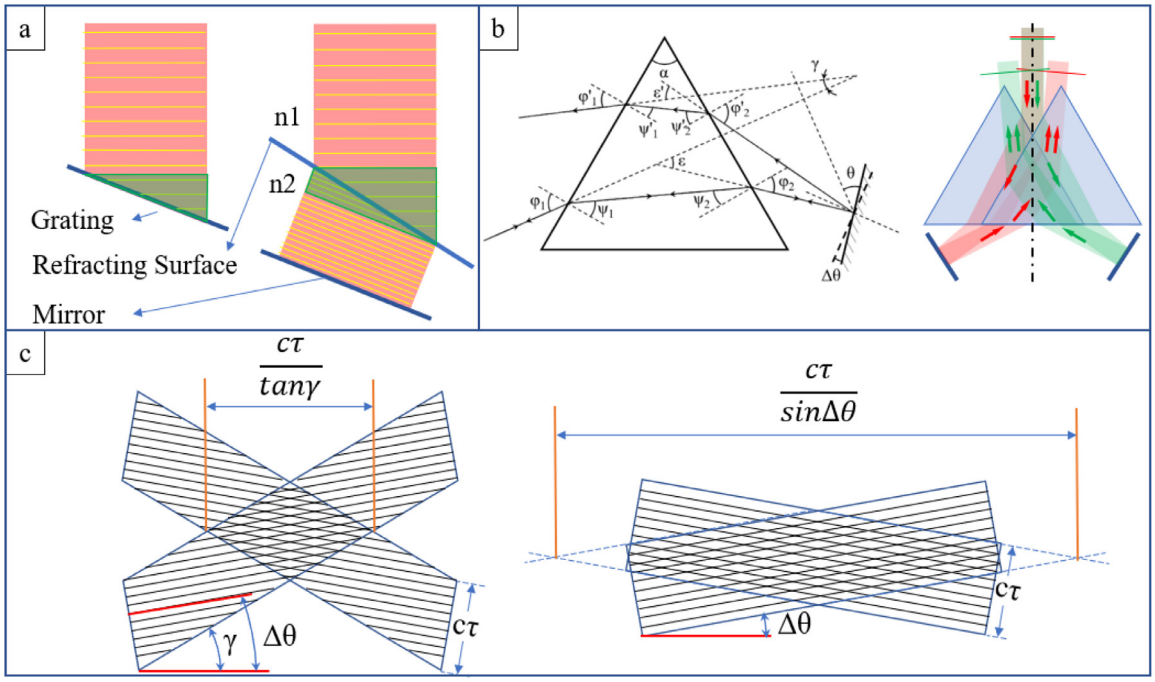

Fig. 4. (a) Differences in OPD in grating-based and prism-based SHS. Monochromatic light incident at Littrow angle to the reflective grating or the dispersion system composed of refractive surface and mirror. The yellow lines mean wavefronts. (b) The dispersion of monochromatic light incident to the prism-mirror in the orthogonal TSHS at non-Littrow angle. Left: schematic diagram of prism-mirror pair for constructing spatial heterodyne, where θ is the tuning angle. Right: Two-arm equivalent light path diagram, where red and green represent two-arm beams respectively. (c) The wavefront diagram of the beam with coherent time τ after system dispersion with a larger interference area. Left: when dispersion element is grating, wavefront and energy front separation due to diffraction. Right: when the dispersion element is a prism, the wavefront and energy front are not separated. Black lines represent the wavefront.

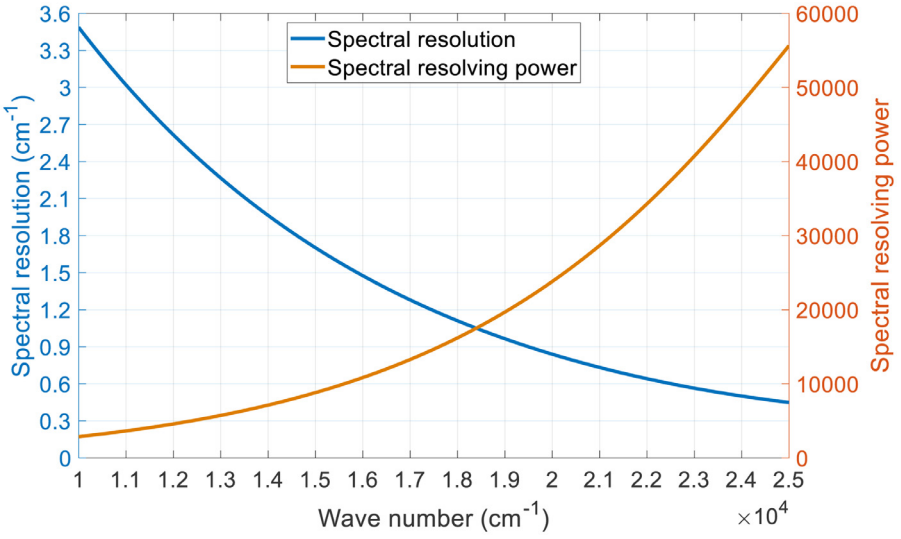

Fig. 5. The relationship curve between spectral resolution / spectral resolution and wavenumber in our setting. The blue line is spectral resolution, and the orange line is resolution power.

when the fringes align on one side of the aperture, on the other side, the minimum intensity of one fringe pattern (s_1) coincides with the maximum intensity of another fringe pattern (s_2). The number of fringes is obtained by dividing the aperture width by fringe spacing. The criterion to distinguish these two wavenumbers is:

$$\frac{w}{s_1} - \frac{w}{s_2} = \frac{1}{2} \tag{5}$$

Accordingly, the spectral resolution R can be obtained as:

$$R = \frac{\sigma_0}{|\Delta\sigma_1 - \Delta\sigma_2|} = \frac{4\sigma_0 s_1 s_2 \sin\gamma_1 \sin\gamma_2}{\left|M\left(s_1 \sin\gamma_1 - s_2 \sin\gamma_2\right)\right|} \tag{6}$$

The dispersion deflection angle γ is related to the prism substrate material, the incident wavenumber σ_i, the tuning angle $\theta_{\sigma 0}$ and the prism incident angle φ_1, so it is difficult to obtain the general function expression of R. To obtain better spectral performance, we choose the equilateral prism with N-SF11 substrate as the dispersion element, and select the Thorlabs AM353T angle mounting frame. Currently, The theoretical incidence angle of prism φ_1=62.8°. By fitting γ, n(σ_i), $\theta_{\sigma 0}$, and σ_i properly, we obtain the relationship curve of the spectral resolution and the number of incident light waves, as shown in Fig. 5. When the prism is used as the dispersion element, the spectral resolution of the instrument is greatly related to the wavenumber, which is due to the nonlinear dispersion characteristics of the prism.

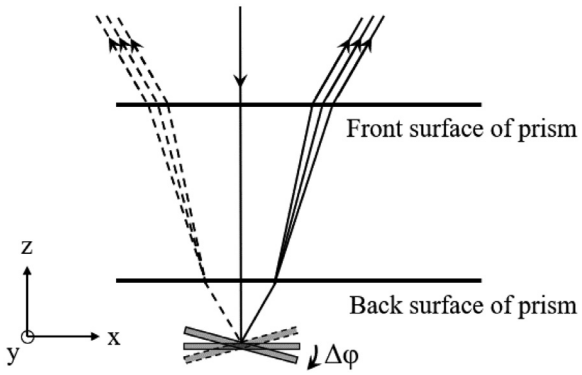

Fig. 6. The plane mirror placed behind the dispersion prism rotates around the y axis to avoid the influence of 'ghost line'. The center of the mirror is defined as the origin, the tuning axis is parallel to the x-axis and passes the origin, the y axis is orthogonal to the tuning axis and parallel to the mirror surface, and the z-axis is perpendicular to the mirror surface. The figure shows the observation of the mirror in the direction perpendicular to the y-axis pre and post rotation of the small angle.

2.4. Ghost line

The reason why the spatial heterodyne spectrometer can make full use of the spatial frequency of the detector is that it is equivalent to moving the Littrow wavenumber to the zero-frequency position, but this will make it difficult to distinguish the spectrum at both ends of the zero-frequency from each other, called "ghost line". For the traditional spatial heterodyne spectrometer, this problem can be solved by setting a band-pass filter, and the cost is that the band range is only half of the theoretical value. But this method is difficult to apply in TSHS. Therefore, TSHS instruments usually solve the "ghost line" problem by adding a fixed frequency in the direction perpendicular to the interference fringe.

For SHS instruments based on diffraction gratings, the frequency in the orthogonal direction is usually introduced by rotating the grating around its vertical axis at a small angle [15]. However, for the SHS instrument based on a dispersion prism, if the dispersion prism is rotated, the refraction angle in the dispersion direction will change, which will affect the accuracy of the recovery spectrum. Therefore, we consider turning the plane mirror behind the dispersive prism around the axis y at a small angle, as shown in Fig. 6. For ease of understanding, the fixed dip angle $\Delta\varphi$ is exaggerated.

When the prism is observed perpendicular to the y axis, it can be equivalent to a parallel plate, and the incident light is perpendicular to the parallel plate, the angle of the incident light is only related to the fixed angle $\Delta\varphi$ currently. And the y-axis is orthogonal to the x-axis, that is, orthogonal to the tuning axis, thus the fixed inclination angle $\Delta\varphi$ will not affect the dispersion angle. Assuming that the transverse wavefront angle of the two-arm beams is $\gamma_{\perp}$, the interference fringes collected by the detector are modulated by the fixed dip angle $\gamma_{\perp}$ in the orthogonal direction, which is equivalent to the whole original spectrum shifting $\Delta\sigma_{\perp}$ in the orthogonal direction. Define $\sigma_x=\sigma-\sigma_L$, $\sigma_y=\sigma_{\perp}$, then

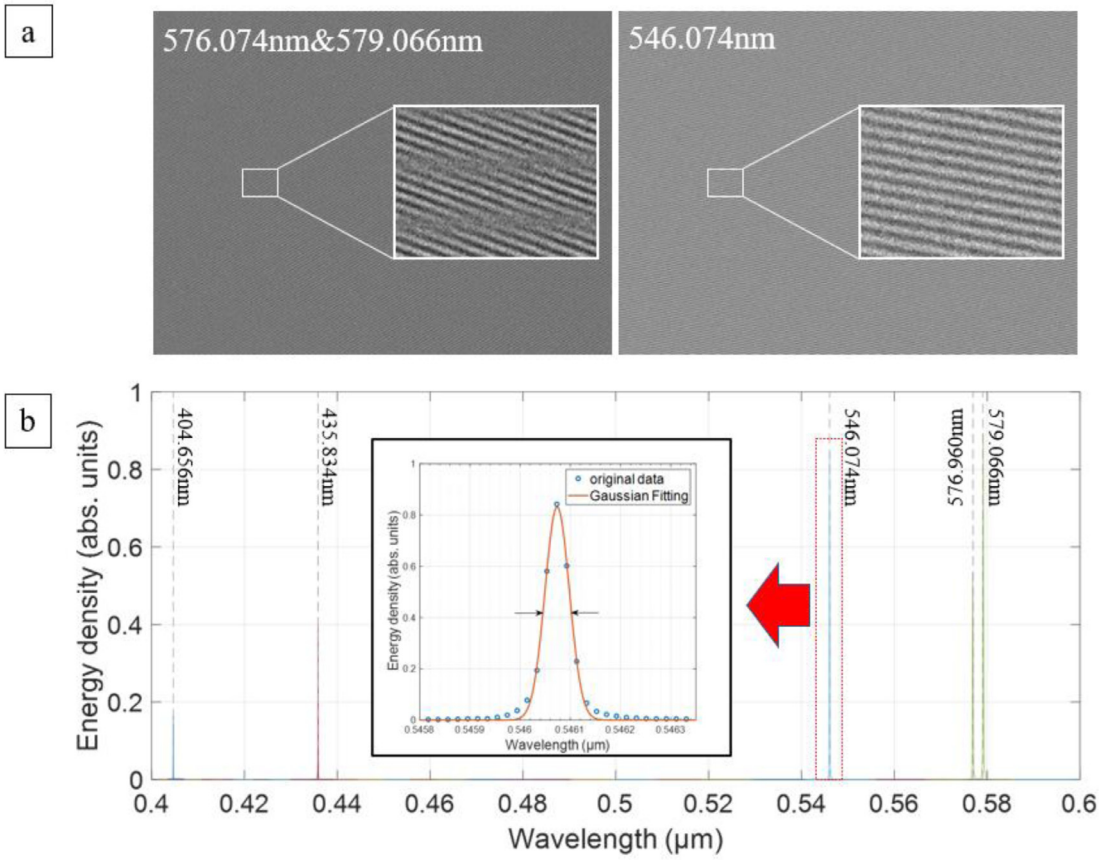

Fig. 7. Part of interferograms and the recovery spectrum of the low-pressure mercury lamp. (a) Interference pattern processed by flat field (Left: 576.960nm & 579.066nm; Right: 546.074nm). (b) The dotted lines are the theoretical position of the spectral line, and the solid lines of different colors represent the data obtained at different tuning angles. The FWHM and theoretical spectral resolution of the recovered spectrum were 0.017nm(0.0075nm), 0.024nm(0.011nm), 0.067nm(0.032nm), 0.078nm(0.040nm), 0.079nm(0.041nm), respectively. The FWHM of the restored spectrum was about twice the theoretical spectral resolution.

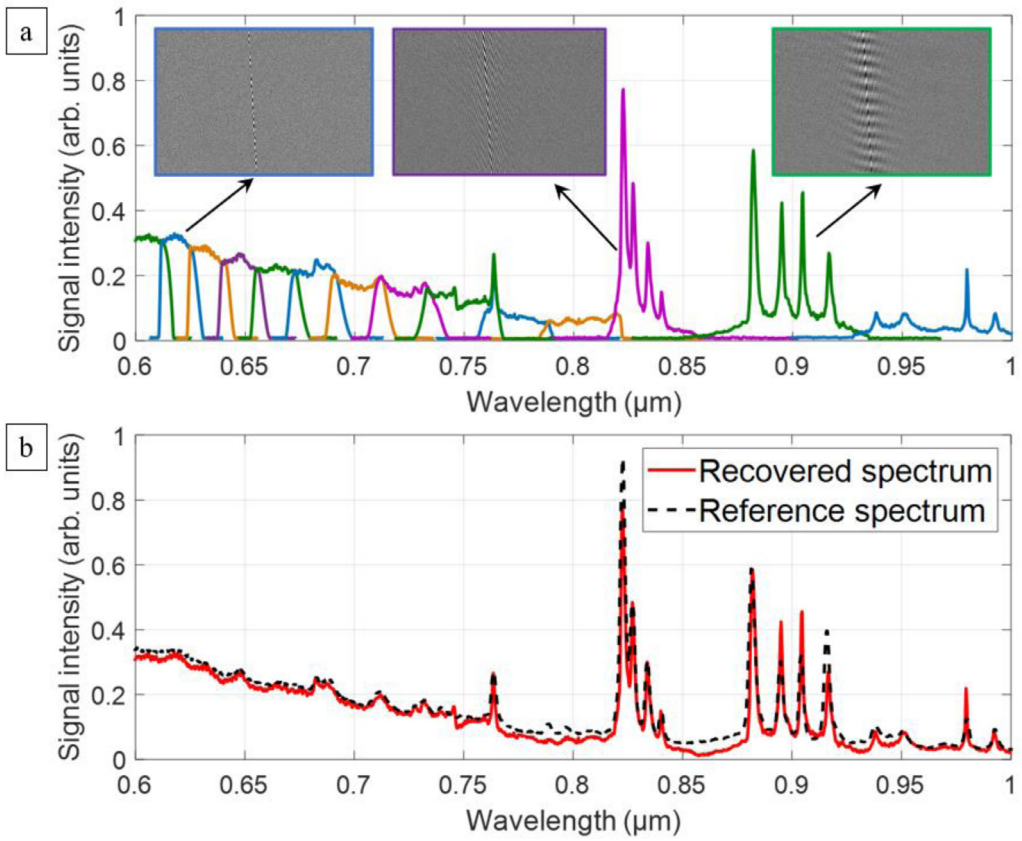

Fig. 8. (a) The Xenon lamp spectrum recovered in the range of 600nm–1000nm, the solid lines of different colors represent the data obtained at different tuning angles. Subgraphs are original interferograms corresponding to different spectral fragments. (b) Comparison of the recovered spectrum and the reference spectrum. The red line is the recovered spectral data after splicing, and the dotted line is the measurement data of marine optical USB4000.

the interferogram can be expressed as:

$$f(\sigma_x, \sigma_y) = \frac{1}{2}[\delta(\sigma_x \mp \Delta\sigma) \times \delta(\sigma_y - \Delta\sigma_\perp) + \delta(\sigma_x \pm \Delta\sigma) \times \delta(\sigma_y + \Delta\sigma_\perp)] \quad (7)$$

The formula (7) shows that when the fixed dip angle $\Delta\varphi$ is zero, the inverse Fourier transform of the same heterodyne wave number on both sides of the Littrow wavenumber is the same, which is the so-called 'ghost line'. If the fixed dip angle is not zero, when the incident light wave number $\sigma > \sigma_L$, the recovered spectrum is in the first and third quadrants of the x0y plane; when the incident light wave number $\sigma < \sigma_L$, the recovered spectrum is in the second and fourth quadrants of the x0y plane, thus separating the aliasing lines and removing the 'ghost line'.

3. Spectral property

In the orthogonal TSHS based on the prism proposed in this paper, the key to realizing the design of a single dispersion element is to introduce the ridge reflector and make the radial surface of the tuning shaft orthogonal to the folding-path plane, the key to avoiding the limitation of lateral interference is to use the prism-reflector instead of the grating to construct the spatial heterodyne. To verify that the proposed technology can be used as a general spectrometer to achieve the measurement of continuous-spectrum targets while maintaining the super-high spectral resolution of SHS, we used a low-pressure mercury spectral lamp and xenon lamp as light sources for spectral reconstruction experiments.

In our setup, the substrate material of the dispersion prism is N-SF11, the actual incident angle φ_1 is 66.923°, the magnification of the bi-telecentric imaging system is 0.5 ×, and the detector resolution is 1440 × 1080 (SONY IMX 273). Based on this, the spectral resolution of the instrument in the range of 405nm ~ 1000nm is about 53471 ~ 2897, that is, the highest spectral resolution is about 7.5pm / 405nm (0.46cm^{-1} / 24691cm^{-1}). The spectral linewidth of mercury lamp is picometer, and the apodization, equilateral dispersion prism alignment error, and other factors will induce the recovery spectral broadening, which induces the spectral resolution of the system lower than the theoretical value. Therefore, the spectral resolution can be characterized by reconstructing the FWHM of the spectral line of the mercury lamp. Part of interferograms and the recovery spectrum are shown in Fig. 7. It should be noted that the current spectral restoration is based on triangular window function.

The system can well recover the characteristic spectral lines in the range of 400 nm–600 nm of a low-pressure mercury lamp, and the spectral performance reached the expected level. However, except for these five spectral lines, other spectral lines are not reflected in the recovered spectrum. This is because the flux of the low-pressure mercury lamp after collimation is very low, and it needs a lot of integration time to collect the interference signal. In this situation, the signal-to-noise ratio is so low that the flat field cannot completely remove the DC (direct current) signal, and then the DC signal will interfere with the recovered spectrum. To avoid this situation, we did not change the integral time in the measurement process.

Taking the sampling interval of 0.2°, the xenon lamp spectra in the range of 600 nm ~ 1000 nm were recovered by 14 measurements. The 14 spectral fragments are shown in Fig. 8a, where different colors represent the data obtained at different tuning angles. It should be noted that Due to the non-linearity of prismatic dispersion, the sampling points of adjacent spectral fragments are not only different but also unequally spaced; at the same time, considering the effect of vignetting, the signal-to-noise ratio of the data on both sides of the single recovered spectrum decreases rapidly, so a part of the data is discarded from the overlapping part of adjacent spectral fragments, and if the difference between the two wave numbers is less than 1/2 times the wave number interval, only the signal at one wave number position is retained, and if the difference between

the two wave numbers is greater than 1/2 times the wave number interval, the signal at both wave number positions is retained. And Fig. 8b is the complete Xenon lamp spectral curve after splicing. The spectrum recovered by our system (red solid line) is in good agreement with the measurement data of USB4000 (black dotted line), which proves that the orthogonal TSHS instrument can be used as a general spectrometer to realize the spectral reconstruction of continuous spectrum targets.

4. Conclusion

We propose a new design of tunable spatial heterodyne spectroscopy (TSHS) based on orthogonal interference optical path, which solves the problem that the existing TSHS cannot guarantee that the OPD between the two arms of the beam along the optical axis is zero in the design of single dispersion element, and truly realizes the design of single dispersion element in TSHS. We also introduce a method of using a prism to construct spatial heterodyne, so as to avoid the problem that the spectral resolution of grating-based spatial heterodyne method decreases when measuring broadband light sources. In addition, we show a 'ghost line' processing method for prismatic spatial heterodyne. The experimental results of a low-pressure mercury lamp and xenon lamp show that the proposed scheme not only has an ultrahigh spectral resolution (up to 53471 of 405 nm) but also can be used as a general spectrometer to measure continuous spectral targets in a wide spectral range (405nm~1000nm). We believe that our work is of great significance to the further development and practical application of TSHS.

Declaration of Competing Interest

The authors declare that they have no known competing financial interests or personal relationships that could have appeared to influence the work reported in this paper

Data availability

Data will be made available on request.

Acknowledgement

This research was support by the National Natural Science Foundation of China (Grant No. 41527806) and the Chinese Academy of Sciences President's International Fellowship Initiative (Grant No. 2021VEA0019). We gratefully acknowledge the assistance of Ivan Syniavskyi in the project.

References

[1] Dohi T, Suzuki T. Attainment of High Resolution Holographic Fourier Transform spectroscopy. Appl Opt 1971;10:1137–40.
[2] Watchorn S, Roesler F, Harlander J, Jaehnig K, Reynolds R, Sanders W. Development of the spatial heterodyne spectrometer for VUV remote sensing of the interstellar medium. In: Proceedings of the international symposium on optical science and technology, 4498. SPIE; 2001.
[3] Englert CR, Brown CM, Bach B, Bach E, Bach K, Harlander JM, Seely JF, Marr KD, Miller I. High-efficiency echelle gratings for MIGHTI, the spatial heterodyne interferometers for the ICON mission. Appl Opt 2017;56:2090–8.
[4] Harlander JM, Roesler FL, Cardon JG, Englert CR, Conway RR. Shimmer: a spatial heterodyne spectrometer for remote sensing of Earth' middle atmosphere. Appl Opt 2002;41:1343–52.
[5] Gornushkin IB, Smith BW, Panne U, Omenetto N. Laser-induced breakdown spectroscopy combined with spatial heterodyne spectroscopy. Appl Spectrosc 2014;68:1076–84.
[6] Palásti DJ, Füle M, Veres M, Galbács G. Optical modeling of the characteristics of dual reflective grating spatial heterodyne spectrometers for use in laser-induced breakdown spectroscopy. Spectrochim Acta Part B At Spectrosc 2021;183:106236.
[7] Fessler KAS, Waldron A, Colón A, Carter JC, Angel SM. A demonstration of spatial heterodyne spectrometers for remote LIBS, Raman spectroscopy, and 1D imaging. Spectrochim Acta Part B At Spectrosc 2021;179:106108.
[8] Harlander JM, Reynolds RJ, Roesler FL. Spatial heterodyne spectroscopy for the exploration of diffuse interstellar emission lines at far-ultraviolet wavelengths. Astrophys J 1992;396:730–40.
[9] Harlander JM, Reynolds RJ, Roesler FL, Li G. Spatial heterodyne spectroscopy: laboratory tests of field-widened, multiple-order, and vacuum ultraviolet systems. In: Proceedings of the EUV, X-Ray, and Gamma-Ray instrumentation for astronomy III. International Society for Optics and Photonics; 1992. p. 48–59.
[10] Egan MJ, Acosta-Maeda TE, Angel SM, Sharma SK. One-mirror, one-grating spatial heterodyne spectrometer for remote-sensing Raman spectroscopy. J Raman Spectrosc 2020;51:1794–801.
[11] Lenzner M, Diels JC. Concerning the spatial heterodyne spectrometer. Opt Express 2016;24:1829–39.
[12] Németh G, Pekker Á. New design and calibration method for a tunable single-grating spatial heterodyne spectrometer. Opt Express 2020;28:22720–31.
[13] Dawson OR, Harris WM. Tunable, all-reflective spatial heterodyne spectrometer for broadband spectral line studies in the visible and near-ultraviolet. Appl Opt 2009;48:4227–38.
[14] Hosseini S, Harris W, Corliss J. Khayyam: a tunable spatial heterodyne spectrometer for observing diffuse emission line targets. In: Proceedings of the ground-based and airborne instrumentation for astronomy IV. SPIE; 2012. p. 1527–37.
[15] Harlander JM, Tran H, Roesler FL, Jaehnig KP, Seo SM, Sanders WT, Reynolds RJ. Field-widened spatial heterodyne spectroscopy: correcting for optical defects and new vacuum ultraviolet performance tests. In: Proceedings of the EUV, X-Ray, and Gamma-Ray instrumentation for astronomy V. International Society for Optics and Photonics; 1994. p. 310–19.